Journal of ELECTRONIC MATERIALS, Vol. 45, No. 2, 2016
DOI: 10.1007/s11664-015-4286-3

Structural, Electrical, and Dielectric Properties of Multiferroic–Spinel Ferrite Composites

MUHAMMAD AAMIR NAZIR,[1] MISBAH UL-ISLAM,[1] IRSHAD ALI,[1] HASSAN ALI,[1] BASHIR AHMAD,[2] SHAHID M. RAMAY,[3] NADEEM RAZA,[2] MUHAMMAD FAHAD EHSAN,[2] and MUHAMMAD NAEEM ASHIQ[2,4,5]

1.—Department of Physics, Bahauddin Zakariya University, Multan 60800, Pakistan. 2.—Institute of Chemical Sciences, Bahauddin Zakariya University, Multan 60800, Pakistan. 3.—College of Science, Physics and Astronomy Department, King Saud University, P.O. Box 2455, Riyadh 11451, Saudi Arabia. 4.—e-mail: naeemashiqqau@yahoo.com. 5.—e-mail: naeembzu@bzu.edu.pk

The present work reports development towards magnetoelectric ceramic composites, i.e., $(1-x)Bi_{0.7}Al_{0.3}Mn_{0.3}Fe_{0.7}O_3$–$xLi_{0.3}Zn_{0.4}Fe_{2.3}O_4$ with x = 0.0, 0.25, 0.35, 0.45, and 1.0. Al- and Mn-doped bismuth multiferroic $Bi_{0.7}Al_{0.3}Mn_{0.3}Fe_{0.7}O_3$ (AMBFO) and Zn-doped lithium ferrite $Li_{0.3}Zn_{0.4}Fe_{2.3}O_4$ (LZF) were synthesized by the coprecipitation and sol–gel method, respectively. The composite system was synthesized by the conventional solid-state reaction technique followed by heat treatment at 700°C for 6 h. X-ray diffraction (XRD) analysis confirmed the formation of orthorhombic and face-centered cubic phase structure in AMBFO and LZF, respectively. The presence of peaks from both systems in the XRD pattern confirmed composite formation. The metal-to-semiconductor transition temperature decreased from 340 K to 330 K with increase in the LZF content, being mainly due to spin canting and phase structure conversion. The direct-current (DC) electrical resistivity was found to be highest for pure AMBFO and then started to decrease with increase in the Li-Zn ferrite (LZF) content in the composites. The dielectric constant decreased with increase in frequency for all samples, in accordance with Koop's phenomenological theory and the Debye relaxation model. However, the alternating-current (AC) conductivity increased with increase in frequency for all samples, which can be attributed to the conduction mechanism of polaron hopping. These composites open a new approach towards magnetoelectric applications, high-frequency devices, and semiconductor-based solar energy conversion systems.

Key words: Composites, dielectric properties, DC resistivity, multiferroics

INTRODUCTION

Recently, materials scientists have shown great interest in development of dielectric ceramic materials with dual properties, i.e., ferroelectricity and ferromagnetism. Multiferroics are materials that exhibit both ferroelectric and ferromagnetic properties in a single phase. However, the magnetization cannot be controlled in a single phase by an electric field, the coupling between the ferromagnetic and ferroelectric is too weak to contribute to large-scale magnetic switching, and most multiferroics also have low Curie temperature.[1] This weak coupling and low Curie temperature result in loss of ferromagnetism or ferroelectricity. Therefore, it is essential to synthesize multiferroic–ferrite composites with high Curie temperature and suitable ferromagnetic–ferroelectric coupling. Based on such development, composite systems can be used to replace multiferroics. In multiferroic–ferrite composites, the magnetization can be easily controlled by applying an electric field, enabling many applications in electronic technology.[2] It has been reported that the

(Received January 20, 2015; accepted December 7, 2015; published online December 28, 2015)

elastic coupling between multiferroics and spinel ferrites may occur through epitaxial or layered alignment. Experimentally, preparation of ferroelectric–ferrite composites that exhibit the magnetoelectric (ME) effect using different techniques has been reported. The ME effect has been investigated in ferroelectric–ferrite composites prepared from both bulk and thin-film multilayer material, i.e., $Pb(Zr,Ti)O_3$–$NiFe_2O_4$ thin films,[3] $BaTiO_3$–$MgFe_2O_4$,[4] $BiFeO_3$–$Li_{0.5}Fe_{2.5}O_4$,[5] and $ZnFe_2O_4$–$BiFeO_3$[6] ceramic composites.

Herein, we report the properties of Al- and Mn-doped $BiFeO_3$ (AMBFO) and Zn-doped Li ferrite (LZF), and the effect of various contents of spinel ferrite in the corresponding composite system. Composites $(1-x)Bi_{0.7}Al_{0.3}Mn_{0.3}Fe_{0.7}O_3$–$xLi_{0.3}Zn_{0.4}Fe_{2.3}O_4$ were synthesized by the solid-state reaction technique. The prepared composite system has many desirable properties linked to suitable applications. The high Curie temperature makes this composite system suitable for use in electronic devices at high temperature. This composite system consists of two ferroics, enabling potential applications in information storage technology. It has a resistivity value suitable for use in microelectronics operating at high frequency. These composite materials also possess low dielectric properties at high frequencies. The high value of the dielectric loss corresponds to large remanent polarization and low leakage current density. The high value of the tangent loss makes them suitable for use in electromagnetic interference components and filter devices.

EXPERIMENTAL PROCEDURES

Chemicals

The chemicals used for synthesis of the multiferroic, zinc-doped lithium ferrite, and their composites were $Li(NO_3)$ (98%, Sigma Aldrich), $Zn(NO_3)_2{\cdot}6H_2O$ (99.5%, Sigma Aldrich), $Fe(NO_3)_3{\cdot}9H_2O$ (98%, Sigma Aldrich), citric acid (99.9%, Fisher Scientific), $Bi(NO_3)_3$ (99%,Merck), $Al(NO_3)_3{\cdot}9H_2O$ (96%, Merck), and $MnCl_2{\cdot}4H_2O$ (99.50%, Sigma Aldrich). All chemicals were used as received without further treatment.

Synthesis of Zinc-Substituted Lithium Ferrite

Li-Zn ferrite (LZF) was synthesized by the chemical sol-gel method. Li-Zn ferrite with formula $Li_{0.3}Zn_{0.4}Fe_{2.3}O_4$ was synthesized by taking stoichiometric amounts of lithium nitrate, zinc nitrate, and ferric nitrate in deionized water. Citric acid solution was added into the above-mentioned metallic salt solutions while keeping the ratio of metals to citric acid at 1:1.5. Citric acid was used as a chelating agent to form complexes with the metal ions and also as a fuel for the combustion process. The pH of the solution was adjusted at 7.0 by using 2 M ammonia solution. The solution was continuously stirred and heated at 80°C to evaporate the solvent. This process was continued until the solution turned into a viscous brown gel, which was then burnt at 300°C and converted into powder. The powder was finally sintered at 800°C in a muffle furnace (VULCAN™ A550) to obtain the required phase.

Synthesis of Al/Mn-Substituted Bi-Based Multiferroic

Al/Mn-substituted multiferroic ($Bi_{0.7}Al_{0.3}Mn_{0.3}Fe_{0.7}O_3$) was synthesized by the chemical coprecipitation method. Solutions of the different metal salts were prepared by taking stoichiometric amounts in deionized water. These solutions were mixed in a beaker, and the mixture was heated up to 60°C on a hotplate with a magnetic stirrer. KOH solution (2 M, used as precipitating agent) was added dropwise under vigorous stirring until the pH of the mixture reached 11 to 12. Brown-colored precipitates were formed during the addition of the precipitating agent. This mixture was stirred for a further 2 h to achieve homogeneity. The precipitates were then washed several times with deionized water until the pH of the filtrate reached 7. These precipitates were dried at 100°C in the oven and finally annealed at 800°C for 7 h in a muffle furnace to obtain the required phase.

Preparation of Composites

Composites with general formula $(1-x)Bi_{0.7}Al_{0.3}Mn_{0.3}Fe_{0.7}O_3$–$xLi_{0.3}Zn_{0.4}Fe_{2.3}O_4$ (x = 0.0, 0.25, 0.35, 0.45, 1.0) were prepared by the solid-state reaction method. Stoichiometric amounts of multiferroic (AMBFO) and ferrite (LZF) were weighed accordingly and mixed. These were ground in an agate mortar and pestle for 5 h to obtain homogeneous powder. Polyvinyl alcohol (PVA) (3% by weight) was added as a binder for the composite system.[7] The mixed powder was dried and pressed into pellets. The composite pellets were finally sintered at 700°C for 6 h.

Characterization

Differential scanning calorimetry (DSC) and thermogravimetric analysis (TGA) of as-prepared Li-Zn ferrite were performed at heating rate of 10°C min^{-1} using an SDT Q600 V8.2 Build 100 analyzer to observe the changes taking place on heating. X-ray diffraction patterns were recorded to confirm the phase of the synthesized materials using a JDX-60PX JEOL Boston model diffractometer operated at 40 kV and 30 mA with a Cu K_α (λ = 1.5418 Å) radiation source. Fourier-transform infrared (FTIR) measurements were performed using a Thermo Scientific Nicolet model 6700 to confirm the x-ray diffraction results and to determine the vibrational modes of various chemical bonds. The direct-current (DC) electrical resistivity

was measured by the two-point probe method using a Keithley model 2400 source meter. The dielectric parameters were measured in the frequency range from 1 MHz to 3 GHz by using an Agilent model E4991 ARF impedance analyzer.

RESULTS AND DISCUSSION

Differential Scanning Calorimetry (DSC) and Thermogravimetric Analysis (TGA)

The thermogravimetric/differential thermogravimetric (TG/DTG) curve for an unannealed sample of Li-Zn ferrite is shown in Fig. 1. The TG curve shows total weight loss of approximately 70%. The weight losses of about 20% at 100°C and 300°C are due to removal of water content and decomposition of citric acid, respectively. The other major weight loss of 50% occurs at 300°C to 620°C, being attributed to formation of oxides of different metals.[8,9] The weight loss curve becomes smooth after 700°C, indicating phase formation. The DTG curve also shows peaks at about 100°C and 300°C corresponding to removal of water and decomposition of citric acid, respectively. The exothermic peak at about 600°C corresponds to formation of different metal oxides, and finally the endothermic peak at 750°C indicates formation of the required phase. Since the TG and DTG curves are in agreement with each other, the final sample was annealed at 800°C to obtain the required spinel phase.

Powder x-ray Diffraction (XRD) Analysis

The x-ray diffraction (XRD) patterns of AMBFO, LZF, and their composites $(1-x)Bi_{0.7}Al_{0.3}Mn_{0.3}Fe_{0.7}O_3$–$xLi_{0.3}Zn_{0.4}Fe_{2.3}O_4$ with compositions x = 0, 0.25, 0.35, and 0.45 at room temperature are shown in Fig. 2. The orthorhombic structure of AMBFO sintered at 800°C and the face-centered cubic structure of lithium zinc ferrite sintered at 800°C belong to space group *Pnma* and *Fd3m*, respectively. The XRD patterns of multiferroic AMBFO are in good agreement with the standard pattern [International Centre for Diffraction Data (ICDD) card no. 86-1518], while the peaks belonging to the Li-Zn ferrite were indexed by the conventional *ab initio* method, also perfectly matching the standard Joint Committee on Powder Diffraction Standards (JCPDS) card no. 008-0234 of the cubic spinel structure. Figure 2 represents the spinel phase of lithium zinc ferrite with *hkl* peaks of (220), (311), (400), (422), and (440) and AMBFO multiferroic with *hkl* of (110), (112), (200), (022), (023), and (400). The presence of peaks for both materials in the composites confirms composite formation. It also indicates the formation of a diphase composite after sintering at 700°C with homogeneous crystallinity. The peaks with Miller indices (110), (112), and (023) belonging to $Bi_{0.7}Al_{0.3}Mn_{0.3}Fe_{0.7}O_3$ do not alter in the composite, while the intensity of the peaks with *hkl* of (220) and (311) belonging to the Li-Zn ferrite increase with increasing ferrite concentration. The

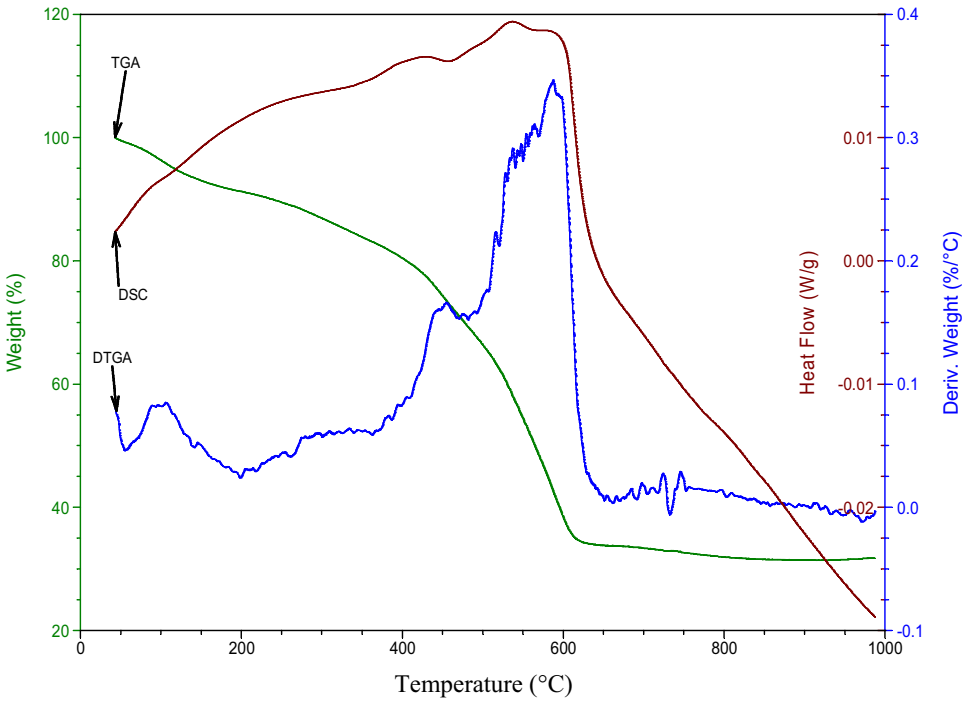

Fig. 1. TGA and DSC curves of as-prepared Li-Zn ferrite.

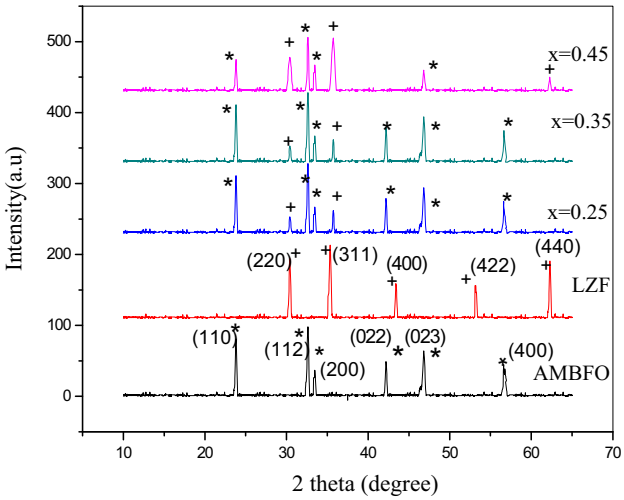

Fig. 2. XRD patterns of (1−*x*)AMBFO–*x*LZF composites with *x* = 0, 0.25, 0.35, 0.45, and 1.0. "*" indicates AMBFO phase; "+" indicates LZF phase.

peak intensity for (110) and (112) decreases while the (022) and (400) peaks belonging to $Bi_{0.7}Al_{0.3}Mn_{0.3}Fe_{0.7}O_3$ disappear at $x = 0.45$.

Fourier-Transform Infrared (FTIR) Spectroscopic Analysis

Figure 3a shows the FTIR spectra for the pure Li-Zn ferrite (LZF) and the composite with $x = 0.45$ in the range from 400 cm^{-1} to 1800 cm^{-1}. The absorption band at 400 cm^{-1} is attributed to stretching vibration of Fe–O bond at octahedral sites, which is common in cubic ferrites.[7] The absorption band at 530 cm^{-1} corresponds to stretching vibration of metal–oxygen (M–O) bonds present at tetrahedral sites of the Li-Zn ferrite. Figure 3b presents the FTIR spectra of $(1-x)Bi_{0.7}Al_{0.3}Mn_{0.3}Fe_{0.7}O_3$–$xLi_{0.3}Zn_{0.4}Fe_{2.3}O_4$ with $x = 0.45$. The spectrum in this range indicates the presence of both cubic and perovskite phases. The absorption band belonging to LZF shifts to 405 cm^{-1}, indicating composite formation. The absorption band at 440 cm^{-1} is attributed to O–Fe–O bending vibration, while the other band at 557 cm^{-1} is due to Fe–O stretching vibration. Both of these broad bands are ascribed to the FeO_6 octahedron of the perovskite structure.[10–12] The shoulder valley at 723 cm^{-1} is associated with stretching vibration of Bi–O bond in the perovskite structure.[13,14] The FTIR results are in good agreement with the x-ray diffraction results.

Direct-Current (DC) Electrical Resistivity

The direct-current (DC) electrical resistivity of the $(1-x)Bi_{0.7}Al_{0.3}Mn_{0.3}Fe_{0.7}O_3$–$xLi_{0.3}Zn_{0.4}Fe_{2.3}O_4$ ceramic composites with $x = 0$, 0.25, 0.35, 0.45, and 1.0 was measured in the temperature range from 25°C to 190°C using the two-point probe method. The resistivity of pure $Bi_{0.7}Al_{0.3}Mn_{0.3}Fe_{0.7}O_3$ and the composites ($x = 0.25$, 0.35, 0.45)

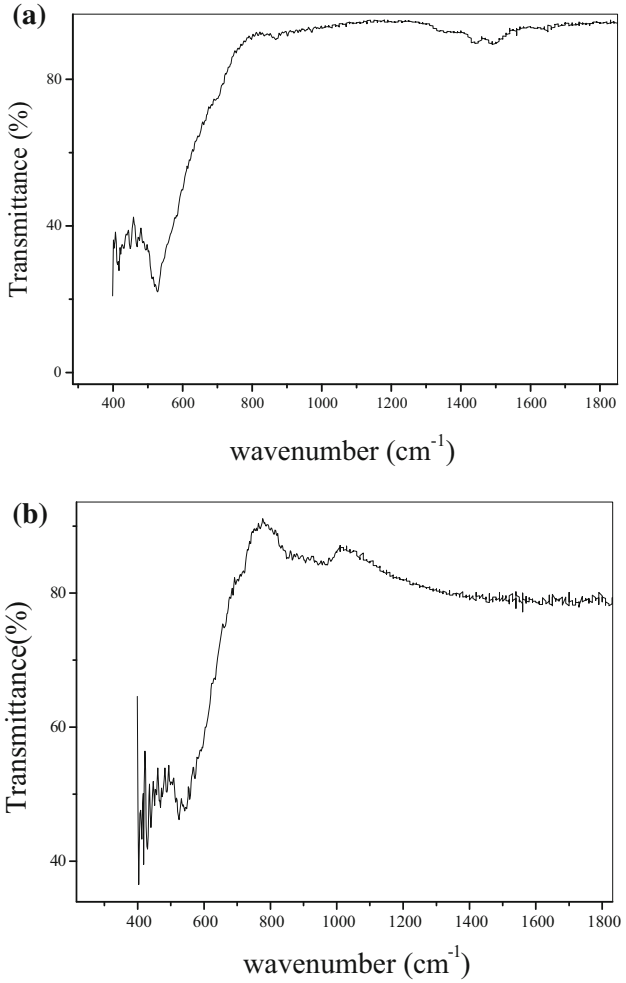

Fig. 3. FTIR spectra of (a) pure LZF and (b) (1−*x*)AMBFO–*x*LZF composite (*x* = 0.5).

increased as the temperature was increased, which is attributed to metallic behavior, attaining a maximum value at a specific temperature, followed by a gradual decrease on further increase in temperature except for pure $Li_{0.3}Zn_{0.4}Fe_{2.3}O_4$ ferrite (with $x = 1.0$), which showed semiconducting behavior, as shown in Fig. 4. The metal-to-semiconductor transition (T_{MS}) in the present investigation is mainly due to spin canting and phase structure conversion.[15] The metal-to-semiconductor transition temperature (T_{MS}) for pure $Bi_{0.7}Al_{0.3}Mn_{0.3}Fe_{0.7}O_3$ is found to be 67°C, while it decreases to 57°C for the composites with $x = 0.25$, 0.35, and 0.45. Different researchers have already reported many other perovskite materials that exhibit metallic behavior at low temperature but semiconducting behavior at high temperature.[10,11,16]

High room-temperature resistivity (1.1×10^9 ohm-cm) is observed for $Bi_{0.7}Al_{0.3}Mn_{0.3}Fe_{0.7}O_3$ due to the substitution of aluminum and manganese. Conduction in the bismuth-based multiferroic (BFO) and lithium zinc ferrite (LZF) is due to hopping of electrons between ferric and ferrous ions

at octahedral sites. Al and Mn both replace iron ions at octahedral site, resulting in a decrease of the iron content at that site as well as the hopping of electrons. As a result, the resistivity of the Al/Mn-substituted material is higher. The room-temperature resistivity for the composites with $x = 0.25$, 0.35, 0.45 showed a decreasing trend with increasing Li-Zn ferrite concentration in $Bi_{0.7}Al_{0.3}Mn_{0.3}Fe_{0.7}O_3$ (Fig. 5). The resistivity for the Li-Zn ferrite is 4×10^7 ohm-cm at room temperature, and its value decreased with rise in temperature, being attributed to its semiconducting behavior as shown in Fig. 4. The proposed basic mechanism of conductivity in ferrites and multiferroics is due to hopping of electrons between different oxidation states of the same elements present at octahedral sites, which can be elaborated as follows:

$$Mn^{2+} + Fe^{3+} \leftrightarrow Mn^{3+} + Fe^{2+} \quad (1)$$

Figure 4 presents a low resistivity value for LZF, which is attributed to the substitution of Li^{1+} ions in place of Fe^{3+} ions at octahedral site; this substitution also pushes the surrounding oxygen ions, resulting in a reduction of the distance between two metal ions at octahedral site and a resultant increase in hopping of electrons, which in turn improves the conductivity. Secondly, the resistivity of the lithium ferrite is lower than that of the AMBFO multiferroic, which is also responsible for the reduction in resistivity of the composites.

The high electrical resistivity of the multiferroic–ferrite composites makes them useful in electronic devices working at high frequencies. Lithium ferrite is also gaining importance because of its high-frequency applications in the microwave to radiofrequency regions. Figure 6 presents a plot of ln ρ versus $10^3/T$, showing linear behavior for all the samples after the transition temperature (T_{MS}); the activation energy was calculated in this region. The high activation energy values found for the Al/Mn-substituted AMBFO and its composites suggest that these materials are suitable for use in solar cells and photovoltaic devices.[10,11]

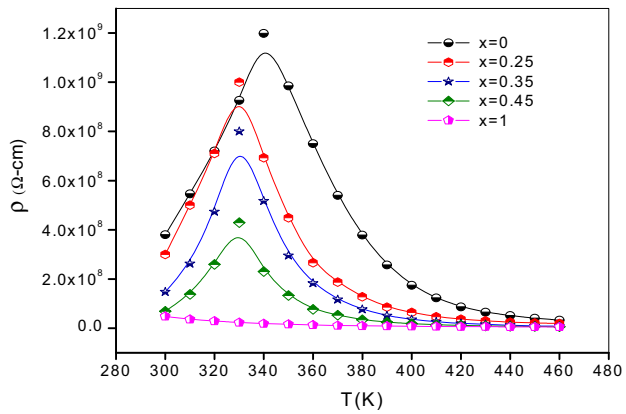

Fig. 4. Variation of DC resistivity with temperature for (1−*x*)AMBFO–*x*LZF composites.

Dielectric Measurements

Dielectric Constant

The change in dielectric constant for all the samples as a function of frequency is shown in Fig. 7. The overall trend is the same for all the samples; i.e., the dielectric constant is high at low frequencies and decreases with increase in frequency. The high value of the dielectric constant at lower frequency is due to interfacial dislocation pile-ups, grain boundaries, and the presence of Fe^{2+} ions. At higher frequency, dipoles will no longer be able to rotate with the frequency, charge carriers lag behind the applied frequency, and transfer of electrons between Fe^{2+} and Fe^{3+} will not follow the AC field. Hence, the polarization decreases with increase in frequency and reaches a constant value,

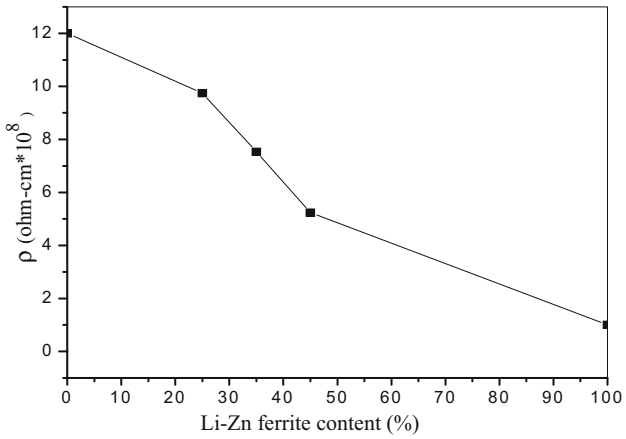

Fig. 5. Variation in DC resistivity versus Li-Zn ferrite content in (1−*x*)AMBFO–*x*LZF composites.

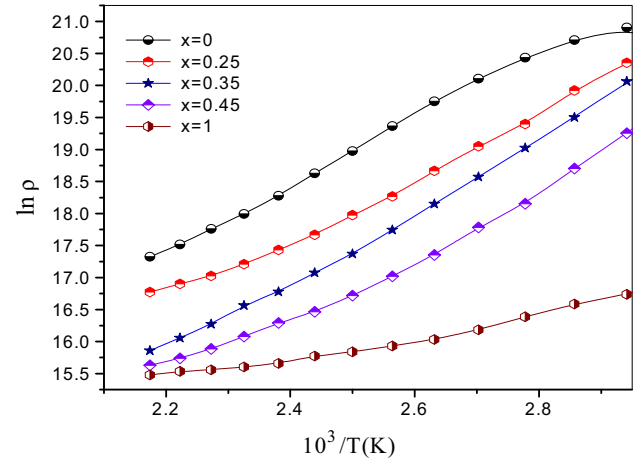

Fig. 6. Plot of ln ρ versus $10^3/T$ for (1−*x*)AMBFO–*x*LZF composites.

giving rise to the relaxation phenomenon up to 1.75 GHz as shown in Fig. 7. This relaxation peak is due to the fact that the exchange of electrons between ferric and ferrous ions no longer follows the applied AC field.

Irregular behavior of the dielectric dispersion occurs at still higher frequencies of approximately 2.5 GHz. At this frequency, atomic or ionic polarization ceases and only electronic polarization is significant. Dispersion is observed in all the samples at 2.5 GHz and higher frequencies, thus giving rise to the resonance phenomenon. The resonance phenomenon is observed at 2.5 GHz when the shifting frequency between Fe^{2+} and Fe^{3+} becomes equal to the applied AC frequency, resulting in the maximum power absorption responsible for the resonance peak.

The dielectric constant slightly decreased with increasing Li-Zn ferrite (LZF) content in the composites at room temperature. However, the resonance peaks became flatter with increasing Li-Zn ferrite (LZF) content. This implies that the dielectric response tends to change from resonance to relaxation. It is clear from Fig. 7 that the resonance peaks became flatter and shifted to slightly higher frequency with increase of the Li-Zn ferrite (LZF) content. This shift corresponds to the increase in the hopping of electrons between elements in different oxidation states, i.e., Fe^{2+} to Fe^{3+} and Mn^{2+} to Mn^{3+}.[17,18]

Dielectric Loss

Figure 8 shows the variation of the dielectric loss as a function of frequency (1 MHz to 3 GHz). At a frequency of 100 MHz, the values of the dielectric loss for the $(1-x)$AMBFO–xLZF composites (x = 0.0, 0.25, 0.35, 0.45, and 1.0) were found to be 0.26, 0.19, 0.10, and 0.10, respectively. Such low values of dielectric loss at 100 MHz correspond to large remanent polarization and low leakage current density. Similar types of results have already been reported in literature.[19] Figure 9 shows a dramatic increase in the dielectric loss in all the samples with increase in frequency. However, in pure AMBFO and the composites (x = 0.25, 0.35, 0.45), the value of the dielectric loss increases rapidly as the frequency is increased above 100 MHz. This is due to dipole resonance, the high value of the resistivity, and the difference between the top and bottom of electrodes.

The value of the dielectric loss for pure AMBFO and the composites (x = 0.25, 0.35, 0.45) is higher than for Li-Zn ferrite, in accordance with Debye relaxation theory.[19] As compared with pure Li-Zn ferrite, this high value of the dielectric loss is because of the heterogeneous distorted structure of AMBFO, the high value of resistivity, and energy dissipation due to internal friction of dipoles. Composites (x = 0.25, 0.35, 0.45) also introduce additional interfaces and friction between the dipoles that result in greater heating loss at high frequency. This heat energy is absorbed by the dielectric and is proportional to the dielectric loss. Consequently, the dielectric loss is also known as the loss factor or dissipation factor.[20]

Tangent Loss

The variation of the dielectric tangent loss in the frequency range from 1 MHz to 3 GHz is shown in Fig. 9. The value of the tangent loss also increases with increase in frequency for all the synthesized materials. This increase in the tangent loss is because of dipole defects, extra interface polarization, and imperfections in the crystal structure.[21] The dielectric tangent loss ($\tan\delta$) is directly related to the dielectric loss (ε'') by the relation in Eq. 2[21]:

$$\varepsilon'' = \varepsilon' \tan\delta. \qquad (2)$$

High resonance peaks are observed for pure AMBFO and the composites (0.25, 0.35, 0.45) at a

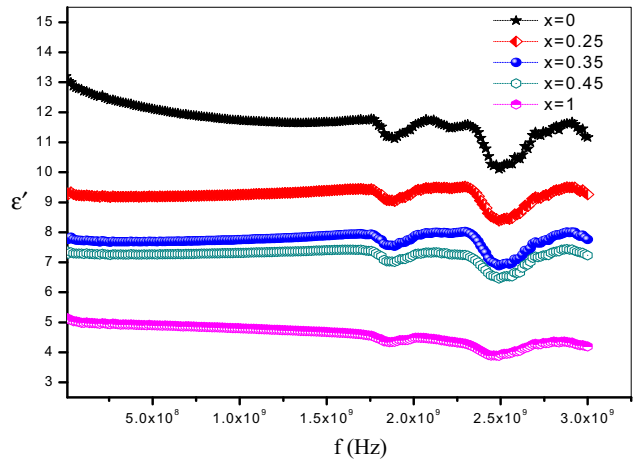

Fig. 7. Variation of dielectric constant with frequency for $(1-x)$AMBFO–xLZF ceramic composites.

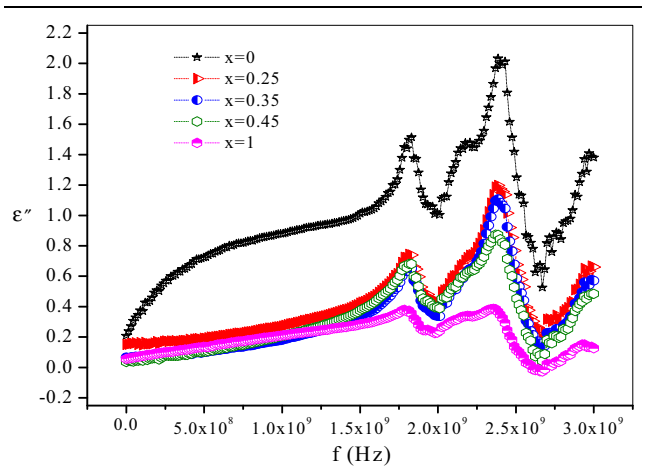

Fig. 8. Effect of frequency on dielectric loss of $(1-x)$AMBFO–xLZF composites.

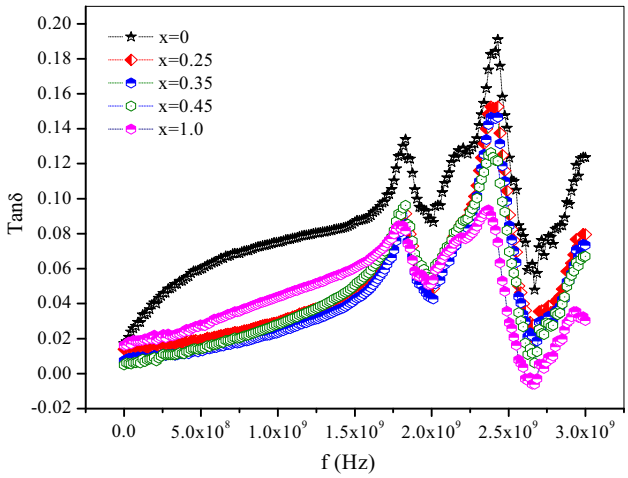

Fig. 9. Effect of frequency on tangent loss of (1−*x*)AMBFO–*x*LZF composites.

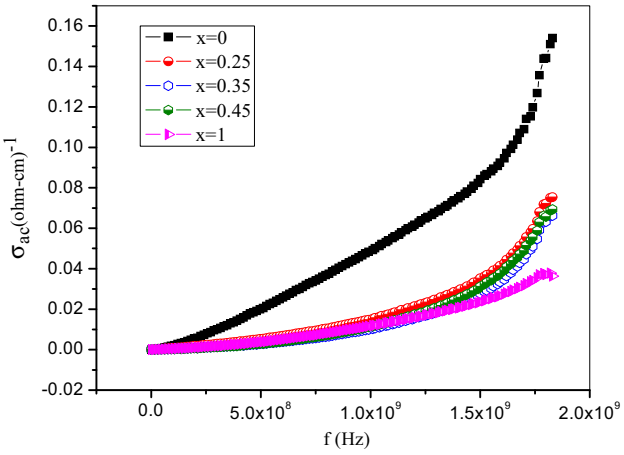

Fig. 10. Variation of AC conductivity with frequency for (1−*x*)AMBFO–*x*LZF composites at room temperature.

frequency of 1.75 GHz. These high values of the dielectric loss and tangent loss make these composites suitable for application in electromagnetic interference (EMI) components and filter devices.[17,22]

AC Conductivity

The AC conductivity (σ_{AC}) was calculated from the following relation:

$$\sigma_{AC} = \omega\varepsilon'\varepsilon''\tan\delta. \quad (3)$$

The AC conductivity of all the samples in the frequency range from 1 MHz to 3 GHz is shown in Fig. 10. The AC conductivity increased with increase in frequency of the applied field, as shown in this figure. This increasing trend of the AC conductivity is due to increase in the hopping of electrons between Fe^{2+} and Fe^{3+} ions present at octahedral sites in both the AMBFO and Li-Zn ferrite, and is strongly frequency dependent.

CONCLUSIONS

XRD and FTIR analyses confirmed that composites of Bi-based multiferroic with lithium-zinc spinel ferrite were successfully prepared. The Al/Mn-substituted multiferroic and all the composite materials showed a metal-to-semiconductor transition which may be helpful in switching applications. The DC electrical resistivity and activation energy decreased with increase in the ferrite content in the composites. The high resistivity of the composites compared with the ferrite makes them useful in microwave devices, as such devices require highly resistive materials. The dielectric parameters decreased with increase in frequency and showed resonance behavior. The dielectric loss and tangent loss of the composite materials were higher than for the multiferroic material. These high values of dielectric loss and tangent loss make these composites suitable for application in electromagnetic interference (EMI) components and filter devices.

ACKNOWLEDGEMENTS

Muhammad Aamir Nazir is highly grateful to the Higher Education Commission (HEC) of Pakistan for financial support under Project No. 20-1515/R&D/09-8049. Shahid M. Ramay would like to extend sincere appreciation to the Deanship of Scientific Research at King Saud University for funding this Research Group (No. RG 1435-004).

REFERENCES

1. M.J. Fiebig, *Phys. D: Appl. Phys.* R123, 38 (2005).
2. Y.K. Fetisov, *Bull. Russ. Acad. Sci. Phys.* 71, 1626 (2007).
3. H. Ryu, P. Murugavel, J.H. Lee, S.C. Chae, T.W. Noh, S. Yoon, H.J. Kim, K.H. Kim, J.H. Jang, M. Kim, C. Bae, and J.G. Park, *Appl. Phys. Lett.* 89, 102907 (2006).
4. S.Y. Tan, S.R. Shannigrahi, S.H. Tan, and F.E.H. Tay, *J. Appl. Phys.* 103, 094105 (2008).
5. R. Rani, J.K. Juneja, S. Singh, K.K. Raina, and C. Prakash, *Adv. Mater. Lett.* 5, 229 (2014).
6. P. Uniyal and K.L. Yadav, *J. Alloys Compd.* 492, 406 (2010).
7. C.E. Ciomagaa, M. Airimioaei, V. Nica, L.M. Hrib, and O.F. Caltun, *J. Eur. Ceram. Soc.* 32, 3325 (2012).
8. M.J. Iqbal and M.N. Ashiq, *Chem. Eng. J.* 136, 383 (2008).
9. K.K. Mallick and J. Roger, *J. Eur. Ceram. Soc.* 27, 2045 (2007).
10. A. Azam, A. Jawad, A.S. Ahmed, M. Chaman, and A.H. Naqvi, *J. Alloys Compd.* 509, 2909 (2011).
11. A.A. Zaky, *Dielectric Solids* (London: Routledge and Kegan Paul, 1970).
12. S. Chauhan, M. Arora, P.C. Sati, S. Chhoker, S.C. Katyal, and M. Kumar, *Ceram. Int.* 39, 6399 (2013).
13. R.K. Mishra, D.K. Pradhan, R.N.P. Choudhary, and A. Banerjee, *J. Phys. Condens. Matter* 20, 045218 (2008).
14. S.G.V. Rao and C.N.R. Rao, *Appl. Spectrosc.* 24, 436 (1970).
15. M.J. Iqbal, M.N. Ashiq, P.H. Gomez, and J.M. Munoz, *J. Magn. Magn. Mater.* 320, 881 (2008).

16. Z. Wang, M. Okude, M. Saito, S. Tsukimoto, A. Ohtomo, M. Tsukada, M. Kawasaki, and Y. Ikuhara, *Nat. Commun.* 1, 106 (2010). doi:10.1038/ncomms1111.
17. B. Ahmad, A. Mahmood, M.N. Ashiq, M.A. Malana, M.N. Haq, M.F. Ehsan, M.F. Warsi, and I. Shakir, *J. Alloys Compd.* 590, 193 (2014).
18. M. Atif, M. Nadeem, R. Grossinger, and R.S. Turtelli, *J. Alloys Compd.* 509, 5720 (2011).
19. G. Dong, G. Tann, W. Liu, A. Xia, and H. Ren, *Ceram. Int.* 40, 1919 (2014).
20. X. Liu, Z. Xu, X.Y. Wei, and X. Yao, *J. Am. Ceram. Soc.* 93, 1245 (2010).
21. A.R. Makhdoom, M.J. Akhtar, M.A. Rafiq, and M.M. Hassan, *Ceram. Int.* 38, 3829 (2012).
22. Y.B. Feng, T. Qiu, and C.Y. Shen, *J. Magn. Magn. Mater.* 318, 8 (2007).